Monthly Notices
of the
ROYAL ASTRONOMICAL SOCIETY

MNRAS **480,** 2466–2474 (2018)
Advance Access publication 2018 July 20

doi:10.1093/mnras/sty1951

Modelling synthetic atmospheric turbulence profiles with temporal variation using Gaussian mixture model

Peng Jia,[1,2]★ James Osborn,[2]★ Letian Kong,[1] Douglas Laidlaw,[2] Caifeng Li,[1] Ollie Farley[2] and Gang Xue[1]

[1]*College of Physics and Optoelectronics, Taiyuan University of Technology, Taiyuan 030024, China*
[2]*Department of Physics, Durham University, South Road, Durham DH1 3LE, UK*

Accepted 2018 July 19. Received 2018 July 19; in original form 2018 June 6

ABSTRACT

The atmospheric turbulence profile plays a very important role for performance evaluation of wide-field adaptive optic systems. Since the atmospheric turbulence is evolving, the turbulence profile will change with time. To better model the temporal variation of turbulence profile, in this paper, we propose to use the extensive stereo-SCIDAR turbulence profile dataset from one observation site to train a Gaussian mixture model. The trained Gaussian mixture model can describe the structure of the turbulence profile in that particular site with several multi-dimensional Gaussian distributions. We cluster the turbulence profile data with the Gaussian mixture model and analyse the temporal variation properties of the clusters. We define the characteristic time as the time that the measured turbulence profile remains in a given profile. We find that normally the characteristic time is around 2 to 20 min and will change at different sites and in different seasons. With the statistical results of the characteristic time and the trained Gaussian mixture model, we can generate synthetic artificial turbulence profiles with realistic temporal variation to better test the performance of adaptive optics systems.

Key words: atmospheric effects – instrumentation: adaptive optics – methods: data analysis – site testing.

1 INTRODUCTION

The Earth's atmospheric turbulence limits the observation ability of ground-based optical telescopes. Adaptive optic (AO) systems are able to compensate the atmospheric-turbulence-induced aberrations in real-time (Babcock 1953). However, due to the isoplanatic angle of the atmospheric turbulence, the correction is effective only in a very small field of view. To obtain a wider field of view with AO correction, several wide-field AO concepts are proposed, such as the multiconjugate adaptive optics (MCAO), ground-layer adaptive optics (GLAO), multi-object adaptive optics (MOAO), and laser-tomography adaptive optics (LTAO). These wide-field AO systems are designed with the assumption that the atmospheric turbulence is a continuous and random media and can be measured and modelled as multiple discrete layers (Tyson 2010).

Measurements of atmospheric turbulence along the vertical direction are expressed as turbulence profiles (TPs). The TP is decomposed into several layers where each layer contains some or all of the following parameters: the height, the magnitude (quantified with the refractive index structure function C_n^2), the wind speed, and the wind direction of the atmospheric turbulence.

The TP is very important for AO modelling and performance analysis (Tokovinin et al. 2005; Tokovinin & Travouillon 2006; Schöck et al. 2010). Depending on the specific wavefront measurement, reconstruction, and deformable mirror control methods in wide-field AO systems, the requirements of TP information are different. However, a basic description of the TP is necessary for both design and performance evaluation of wide-field AO systems.

Generally, the TPs used by the AO community are specific TPs generated directly from measurement data through statistical methods. This model is static and cannot reveal the temporal variation of TPs. With a statistic model, it is hard to evaluate AO system performance in the time domain (such as in different seasons, days. or different hours in one night). The static model also brings difficulties in modelling wide-field AO system through Monte Carlo simulation to test, for example new reconstructor or controller design (Wang, Gilles & Ellerbroek 2011; Costille & Fusco 2012; Kulcsár et al. 2012; Martin et al. 2012; Gilles et al. 2013; Correia et al. 2014; Gendron et al. 2014; Osborn et al. 2014; Ono et al. 2016).

Evaluation AO system with detailed TP temporal variation is very important both for scientific observation strategy plan and post-processing algorithm design. For example, a detailed point spread

★ E-mail: robinmartin20@gmail.com (PJ); james.osborn@durham.ac.uk (JO)

function reconstruction algorithm can provide point spread function model for each 'epoch' of AO observation (Tuan et al. 2018) as PSF model for WFC3/IR in *HST* (Anderson 2016). Besides, we can also evaluate AO performance with a more realistic model. Although direct evaluation of the AO performance with all measurement data is possible, but it is time-consuming even for the simplest wide-field AO systems (Tokovinin 2004). As more and more TP measurements are carried out at different sites, huge amount of TP data are obtained (Schöck et al. 2009; Sarazin et al. 2013; Liu et al. 2015; Osborn et al. 2016). For example, the recent Stereo-SCIDAR Campaign of Paranal (2018A release) has produced over 10 000 profiles covering 83 nights of operation (Osborn et al. 2018). The large amount of TP data makes it possible to describe the real distribution of TPs in the time domain with a probabilistic model.

In this paper, we propose to use a Gaussian Mixture Model (GMM) to describe TP temporal variation. Using the GMM, we can describe the temporal variation of the TPs. Then, we are able to generate synthetic TPs with specific temporal variation for Monte Carlo simulation of AO systems. The method proposed in this paper, along with realistic atmospheric turbulence phase screen generation (Jia et al. 2015a,b; Buscher 2016) and observation real-time simulation methods (Wang 2012), can be used to get high-fidelity simulation of AO (Carbillet et al. 2004; Basden et al. 2007; Le Louarn et al. 2012; Conan & Correia 2014; Basden et al. 2018). We can also use this method for AO concept testing (Zhang, Guo & Rao 2017), observation strategy design (Jia, Basden & Osborn 2018), even modelling (Peterson et al. 2015) and analysing point spread function (PSF) temporal variation in sky surveying telescopes (York et al. 2000; Ivezic et al. 2008; Dark Energy Survey Collaboration et al. 2016), such as SDSS PSF study carried out by Xin et al. (2018). The GMM model as a description method can be used with other methods (Chen et al. 2016) to help us better analyse the properties of the TP. This paper contains the following parts. In Section 2, we will discuss the theory of the GMM for TPs with temporal variation. In Section 3, we will show how to simulate the TP temporal variation with GMM and in Section 4, we will give our conclusions and anticipate future work.

2 DESCRIPTION OF THE TEMPORAL PROPERTY OF TP WITH GMM

2.1 Gaussian mixture model

The GMM is a type of statistical model which is used to describe an overall population with several sub-populations of data. It is an unsupervised machine learning algorithm and is widely used for data analysis, such as clustering analysis of exoplanet transits, white dwarfs, stellar populations, pulsar, gamma-ray bursts, and spectrum of the interstellar medium (Hao et al. 2009; Shin, Sekora & Byun 2009; Lee et al. 2012; Shang & Oh 2012; Shin et al. 2012; Andrews, Price-Whelan & Agüeros 2014; Zhang et al. 2016; Chattopadhyay & Maitra 2017). The GMM assumes any distribution can be modelled with several Gaussian distributions $N(x|u_k, \Sigma_k)$ with different mean value, u_k, and variance, Σ_k, as shown in equation (1):

$$P(x) = \sum_{k=1}^{m} P_k N(x|u_k, \Sigma_k), \tag{1}$$

where $P(x)$ is the distribution to be modelled and P_k is the weight of the Gaussian distribution $N(x|u_k, \Sigma_k)$ within the whole distribution. For a multidimensional distribution, where $\boldsymbol{x}$ is a vector with length of L, the GMM can be described as equation (2):

$$P(\boldsymbol{x}) = \sum_{k=1}^{m} P_k N(\boldsymbol{x}|\boldsymbol{u_k}, \boldsymbol{\Sigma_k}). \tag{2}$$

Here, $N(\boldsymbol{x}|\boldsymbol{u_k}, \boldsymbol{\Sigma_k})$ is a multidimensional Gaussian distribution and $\boldsymbol{u_k}$ is the mean vector with size of L and $\boldsymbol{\Sigma_k}$ is the covariance matrix with size of $L \times L$ as shown in equation (3):

$$N(\boldsymbol{x}|\boldsymbol{u_k}, \boldsymbol{\Sigma_k}) = \frac{1}{(2\pi)^{n/2}\sqrt{|\boldsymbol{\Sigma_k}|}} \exp[-\frac{1}{2}(\boldsymbol{x} - \boldsymbol{u_k}) \cdot \boldsymbol{\Sigma_k}^{-1} \cdot (\boldsymbol{x} - \boldsymbol{u_k})], \tag{3}$$

where n is the dimension number of the multidimensional Gaussian distribution. Although the GMM is solely based on the Gaussian distribution, it can also model the distribution that is not a mixture of Gaussian distributions (Kelly 2007). This property makes it suitable to describe the whole data set of TPs, since there are not any prior assumptions in the distribution of TPs.

Given a set of TP data $\boldsymbol{x}$ and the GMM model, we can fit the parameters (P_k, $\boldsymbol{u_k}$, and $\boldsymbol{\Sigma_k}$) through many different methods. The expectation maximization (EM) is commonly used. EM uses two estimation steps iteratively to obtain the final parameters as shown in Algorithm 1. In this algorithm, the EM algorithm fits a distribution through two steps: first, it fits the distribution with several Gaussian distributions and then adjusts the parameters of these Gaussian distributions to maximize the estimation.

Algorithm 1 Framework of EM Algorithm for GMM

Require:
The training TP data set $\mathbf{x}$ and the number of the Gaussian distributions (m) in the GMM

Ensure:
P_k, $\mathbf{u_k}$ and $\Sigma_\mathbf{k}$ of each Gaussian distributions in the GMM

1: Initialization the GMM with random value of P_k, $\mathbf{u_k}$ and $\Sigma_\mathbf{k}$
2: E-step (expectation-step): calculate $P(\mathbf{x})$ and $N(\mathbf{x}|\mathbf{u_k}, \Sigma_\mathbf{k})$ with equations 2 and 3
3: M-step (maximization-step): update the parameters P_k, $\mathbf{u_k}$ and $\Sigma_\mathbf{k}$ with:
$\mathbf{u_k} = \frac{\sum_{i=1}^{L} \mathbf{x}_i P_k N(\mathbf{x}_i|\mathbf{u_k}, \Sigma_\mathbf{k})/N(\mathbf{x}_i)}{\sum_{i=1}^{L} P_k N(\mathbf{x}_i|\mathbf{u_k}, \Sigma_\mathbf{k})/N(\mathbf{x}_i)}$
$\Sigma_\mathbf{k} = \frac{\sum_{i=1}^{L} (\mathbf{x}_i - \mathbf{u_k}) \otimes (\mathbf{x}_i - \mathbf{u_k}) P_k N(\mathbf{x}_i|\mathbf{u_k}, \Sigma_\mathbf{k})/N(\mathbf{x}_i)}{\sum_{i=1}^{L} P_k N(\mathbf{x}_i|\mathbf{u_k}, \Sigma_\mathbf{k})/N(\mathbf{x}_i)}$
$P_k = \frac{1}{N} \sum_{i=1}^{L} P_k N(\mathbf{x}_i|\mathbf{u_k}, \Sigma_\mathbf{k})/N(\mathbf{x}_i)$
where $\otimes$ is the outer product
4: **while** The likelihood function $\gamma(\mathbf{x})$ is not converge **do**
5: Repeat step 2 and step 3
6: **end while**

Through minimizing the likelihood function defined by equation (4), GMM is able to model the whole distribution by several Gaussian distributions with different parameters

$$\gamma(\boldsymbol{x}) = \sum_{i=1}^{L} \log \left\{ \sum_{k=1}^{m} P_k N(\boldsymbol{x}_k|\boldsymbol{u_k}, \boldsymbol{\Sigma_k}) \right\}. \tag{4}$$

Before we obtain a particular GMM from the TP data, the number of Gaussian distributions (m) is defined manually. Like all the other model-fitting problems, when m is small, the model will face the underfitting problem. As m increases, we will get better fitting results and will more likely get an overfitting model. To reduce the risk of underfitting and overfitting, we fit the TP data with a GMM of several different Gaussian distributions and use the theoretic-information criteria to select the best number.

Table 1. TP measurements data summary.

Site	Observation Month	Number of Observation Days
Paranal	Jan.	10
	Mar.	3
	Apr.	13
	May.	5
	Jun.	3
	Jul.	12
	Aug.	6
	Nov.	12
	Dec.	19
La Palma	Jun.	6
	Jul.	7
	Sep.	2
	Oct.	12

Because the true statistical model of TP distribution is unknown right now, to reduce the risk of selecting a very bad model, we will choose Akaike information criterion (AIC) defined in equation (5) for model selection as discussed in Vrieze (2012).

$$\mathrm{AIC}(Model) = -2\log\gamma(\boldsymbol{x}, Model) + m \tag{5}$$

where $Model$ is the GMM model with m Gaussian distributions, $\boldsymbol{x}$ is the data set, and $\gamma(\boldsymbol{x}, Model)$ is the likelihood function defined in equation (4). It should be mentioned here that other theoretic-information criteria can also be considered, if further analysis of TP statistical distribution can place other regularization conditions to the GMM.

2.2 Training GMM with TP data

Two sets of TP data are used in this paper: La Palma TP data (Osborn et al. 2015) and Paranal TP data (Osborn et al. 2018). They are both obtained by Stereo-SCIDAR (Shepherd et al. 2014) and the time gap between two adjacent measurements in these data sets is around 1 min. The La Palma TP data set is 15 d of observation data and the Paranal TP data set is 83 d of observation data as listed in Table 1. The total number of TPs is 2880 for La Palma and 10 715 for Paranal.

One measurement of TP data can be seen as a 3D data set with dimension of $4 \times M \times T$. The four dimensions of each TP measurement are height (h), integrated magnitude of the refractive index structure function ($C_n^2 dh$), wind speed (v), and wind direction (θ). M is the number of measurement grids in the vertical direction (100 for all TPs used in this paper) and T is the total number of measurements. The properties of these four dimensions are listed as follows:

(1) the height increases from the observatory altitude to the maximal height (25 000 metre for our data set);
(2) the $C_n^2 dh$ is primarily between 10^{-14} and $10^{-13} m^{1/3}$;
(3) the wind speed is distributed from several to several dozens metres per second;
(4) the wind direction is distributed between 0 to 360 deg.

We normalize the integrated magnitude of $C_n^2 dh$ with equation (6):

$$\overline{C_n^2(h)dh} = \frac{C_n^2(h)dh}{\sum C_n^2(h)dh}, \tag{6}$$

because the $\overline{C_n^2 dh}$ can better reflect the structure of the TP with finite numerical accuracy. The wind speed and direction are hard to measure (Laidlaw et.al. 2018 submitted). Only layers with strong wind speed have effective values of wind speed and direction. Due to this reason, we only use wind speed in this paper and interpolate the wind speed between effective measurements. We will be able to obtain better model, when there are other measurements from balloon-borne radiosonde or weather forecast. An example TP before and after interpolation is shown in Fig. 1.

To model the temporal variation of the whole data set, we will use three dimensions of the TP data for model fitting. Since one measurement $\boldsymbol{x}$ used in this paper is a vector with size of 300 (3×100), the size of data matrix is 300×2880 for La Palma and 300×10715 for Paranal. Although clustering analysis of one dimension in the TP is more useful for some other applications, such as clustering analysis of C_n^2 (Farley et al. submitted), we will transform one measurement from a $3 \times M$ matrix into a vector $\boldsymbol{x}$ of size L as shown in equation (7):

$$\boldsymbol{x} = \left[h_1, h_2, ..., \overline{C_{n_1}^2 dh}, \overline{C_{n_2}^2 dh}, ..., v_1, v_2, ...\right], \tag{7}$$

where h_i..., $\overline{C_{n_i}^2 dh}$... and v_i, ... are values of one TP measurements and they are listed with the height increment order.

As we discussed in Section 2.1, the number of Gaussian distributions needs to be carefully selected to prevent underfitting and overfitting problems. Since the number of Gaussian distributions is an integer and lies between 1 and the maximal dimension (300 for our data), it is possible to find the optimal number through one-dimensional search with AIC as evaluation function. As shown in Fig. 2, the optimal number of Gaussian distributions is 9 for the La Palma data set and 12 for the Paranal data set. With the optimum number of Gaussian distributions, we can train the GMMs using the EM algorithm discussed in Section 2.1.

2.3 TP temporal variation description with GMM

We can get the parameters of the Gaussian distributions in the GMM, after training with the whole data set. Each of these Gaussian distributions can be viewed as a description of a particular cluster and we are able to classify our original TP data set into these different clusters. We labels to these clusters and all the TPs that belong to one of these clusters will be given the same label. Because we have a very high sampling rate of TP in the time domain, it is possible to analyse the temporal variation of TP with its label and observation time.

To obtain the TP temporal variation properties, we first fit each of the TP data, $\boldsymbol{x}$, with Gaussian distributions to the trained GMM as shown in equation (3) and set the label of $\boldsymbol{x}$ as the label of Gaussian distribution with which $\boldsymbol{x}$ has the maximal value. Then, we use equation (8) to calculate the time length within which all the TPs have the same label,

$$\delta t_k = t_{k+n} - t_k, \tag{8}$$

where t_k and t_{k+n} are the time of the first and the last consecutive measurement of TP with the same label, and δt_k is the characteristic time of the TP. The characteristic time is very important for evaluating the temporal variation of TP, it reflects how long the TP can be stable in the space described by the GMM. To reduce the impact brought by non-continuous measurements, we need at least two continuous measurements to calculate the characteristic time. We also delete the characteristic time where the time gap between two adjacent measurements is more than 5 min.

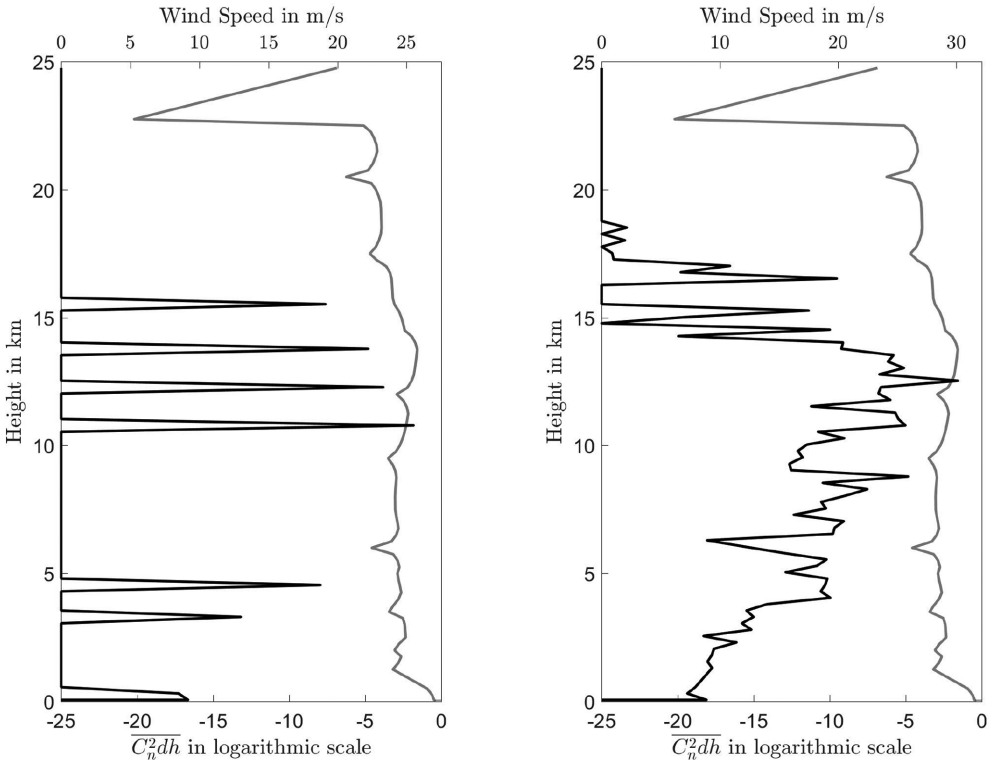

Figure 1. The left-hand panel stands for a TP before interpolation of wind speed and the right-hand panel stands for the same TP after interpolation. The grey line stands for the $\overline{C_n^2 dh}$ in logarithmic scale and the black line stands for the wind speed. In this paper, wind speed from the layers with strong wind speed are used and in several layers there are no wind speed measurements. We use interpolation to solve this problem and the values of wind speed are continuous after interpolation.

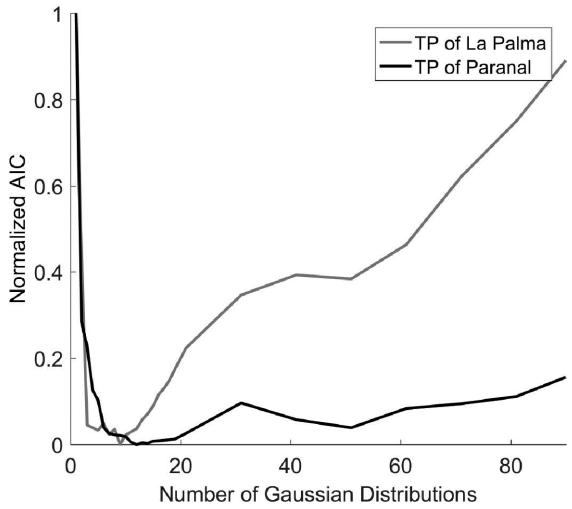

Figure 2. The relation between AIC and the number of Gaussian distributions in GMM for La Palma data set and Paranal data set. The *x*- axis stands for the number of Gaussian distributions and the *y*- axis stands for the normalized information criterion, which is the AIC values normalized by their maximal value, respectively. For La Palma data set, the AIC has its minimal value when the number of Gaussian distributions is 9; for Paranal data set, the AIC has its minimal value when the number of Gaussian distributions is 12. We use 9 and 12 Gaussian distributions for La Palma and Paranal data, respectively. We only show the results of GMM with maximal of 90 Gaussian distributions here for better illustration.

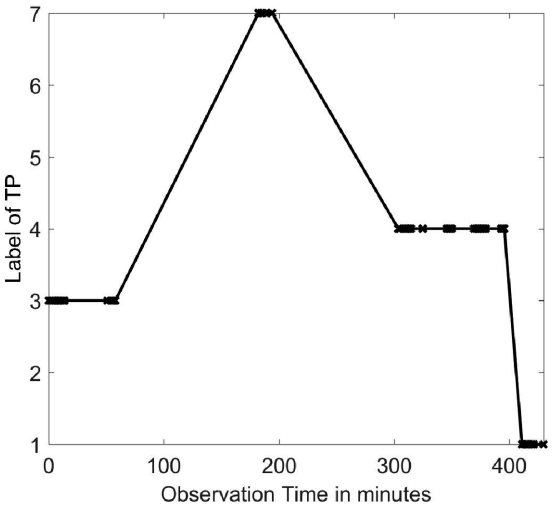

Figure 3. Temporal variation of the TP measurements within the first 420 min from La Palma 2016-06-28. The *x*- axis is the measurement time and the *y*- axis is the label of TP. We can find that the TP will change after several dozens of minutes. The labels of TPs are distributed mainly in 1, 3, 4, and 7 within these 420 min. It indicates that the TP is stable.

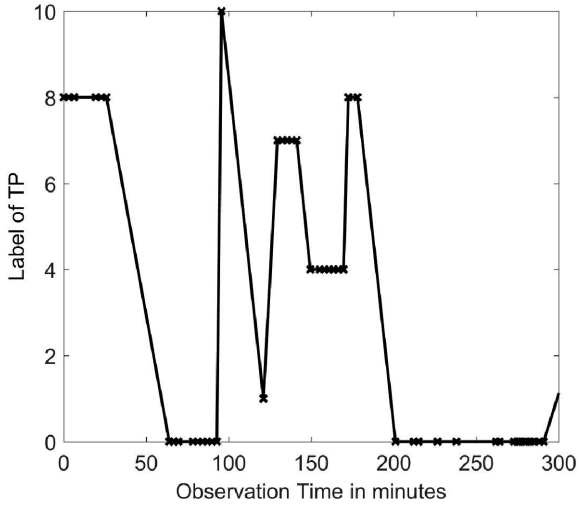

Figure 4. Temporal variation of the TP measurements within the first 300 min from Paranal 2017-04-13. The *x*-axis is the measurement time and the *y*-axis is the label of TP. We find that the TP will change after several minutes. In comparison to Fig.3, the TP changes frequently from 100 to 200 min and becomes stable after that. This phenomenon is common and should be considered for AO performance evaluation.

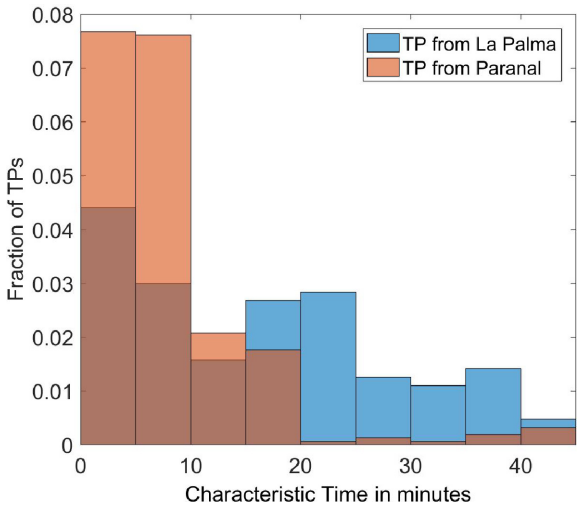

Figure 5. Normalized histogram of characteristic time for La Palma and Paranal. We can find that the characteristic time in Paranal is shorter than that in La Palma.

Table 2. Characteristic time δt (in min) of TP from La Palma and Paranal in min.

Different Site	Mean δt	1st quartile δt	3rd quartile δt
La Palma	21.24	6.01	26.37
Paranal	10.78	2.33	10.80

Table 3. Characteristic time δt (in min) of TP from La Palma in different months.

Month	Mean δt	1st quartile δt	3rd quartile δt
Jun.	27.62	10.43	36.18
Jul.	15.83	5.62	23.01
Sep.	24.38	4.94	28.35
Oct.	25.59	4.50	35.69

Table 4. Characteristic time δt (in min) of TP from Paranal in different months.

Month	Mean δt	1st quartile δt	3rd quartile δt
Jan.	11.17	4.79	11.22
Mar.	9.46	3.52	11.80
Apr.	8.37	2.39	9.67
May.	8.43	4.55	9.30
Jun.	10.92	3.55	8.76
Jul.	10.79	1.89	9.10
Aug.	24.07	3.89	17.92
Oct.	16.20	6.48	11.82
Nov.	7.44	4.48	8.95
Dec.	10.60	6.84	11.62

Two sequences of TPs with temporal variation are shown in Figs.3 and 4. We can find that the TP can vary rapidly on time scales of minutes or more slowly with no changes for several hours.

3 GENERATION OF TP WITH TEMPORAL VARIATION WITH GMM

3.1 Statistical results of TP temporal variation

To better simulate and evaluate AO performance with the GMM TP model, we need to carry out statistical analysis of the characteristic time of different sites and different seasons. The histogram of the characteristic time in La Palma and Paranel is shown in Fig. 5 and some of the statistical results of the characteristic time are shown in Table 2. Because the statistical distribution is not a Gaussian distribution and there are TPs with very long characteristic time, we propose to use the first quartile for the shortest characteristic time estimate and the third quartile for the average characteristic time estimate. We find that, on average, the TP will change within 2–20 min. The temporal variation of TP is almost within the same scale of the temporal variation of PSF in sky surveying telescopes (5-30 min for SDSS as discussed by Xin et al. (2018)). This raises the importance of modelling and analysing the impact of the temporal variation TP to scientific observations.

The temporal variation of the TP can be further analysed to provide a reference for modelling and simulation of the TP in different seasons. The statistical results of the characteristic time in different seasons are shown in Tables 3 and 4. Since there is limited data from these sites, the statistical results reflect limited information. We can glimpse that the TP is more stable in La Palma than that in Paranal.

We can suggest the following conclusions about the TP temporal variation for AO modelling according to the statistical data above:

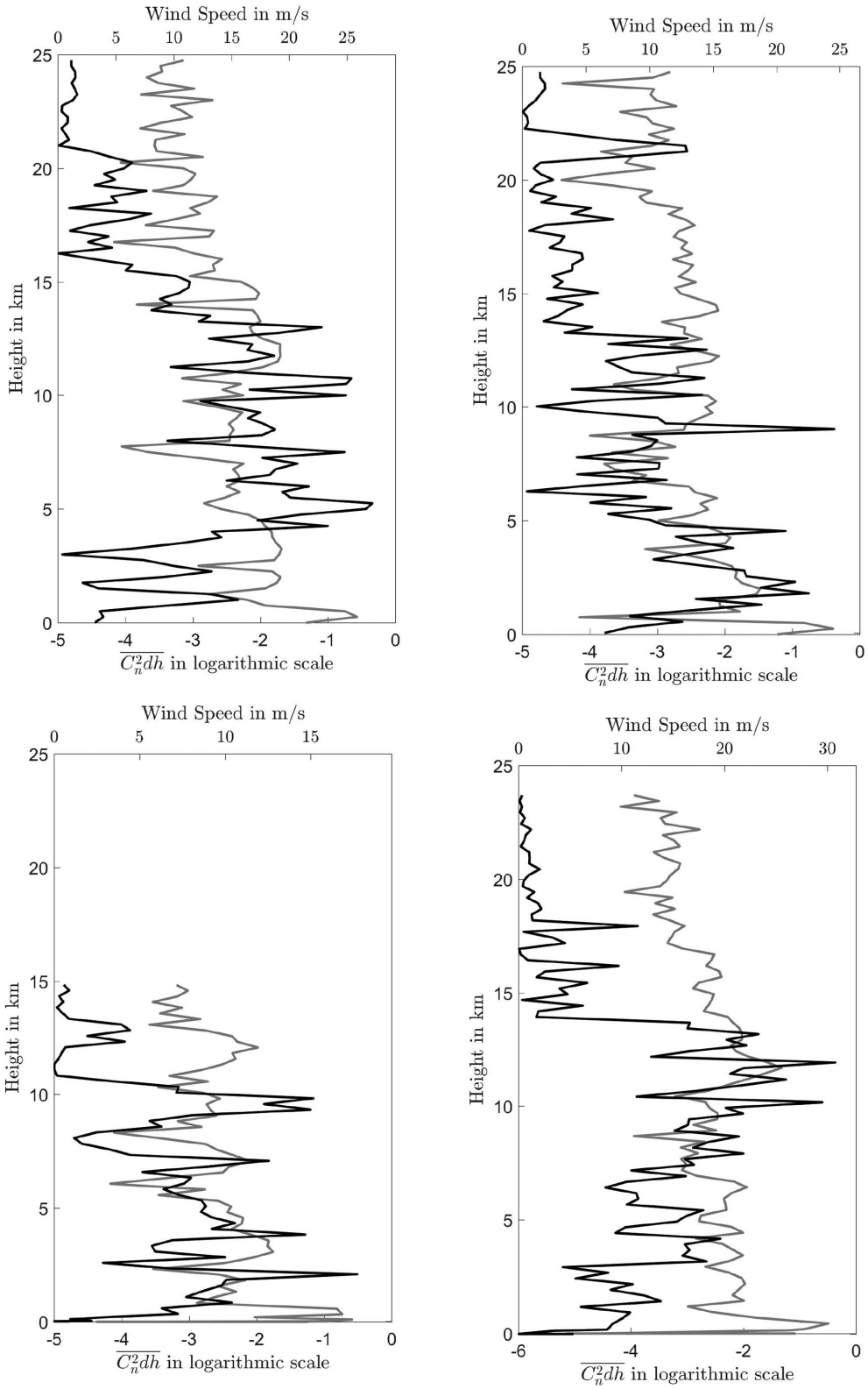

Figure 6. Typical TPs with different labels (from 1 to 4) generated by GMM trained from La Palma Data. The plot in grey is the $\overline{C_{n_i}^2 dh}$ in logarithmic scale and the plot in black is the wind speed. These TPs are listed according to their labels in ascending order from left to right and from top to bottom.

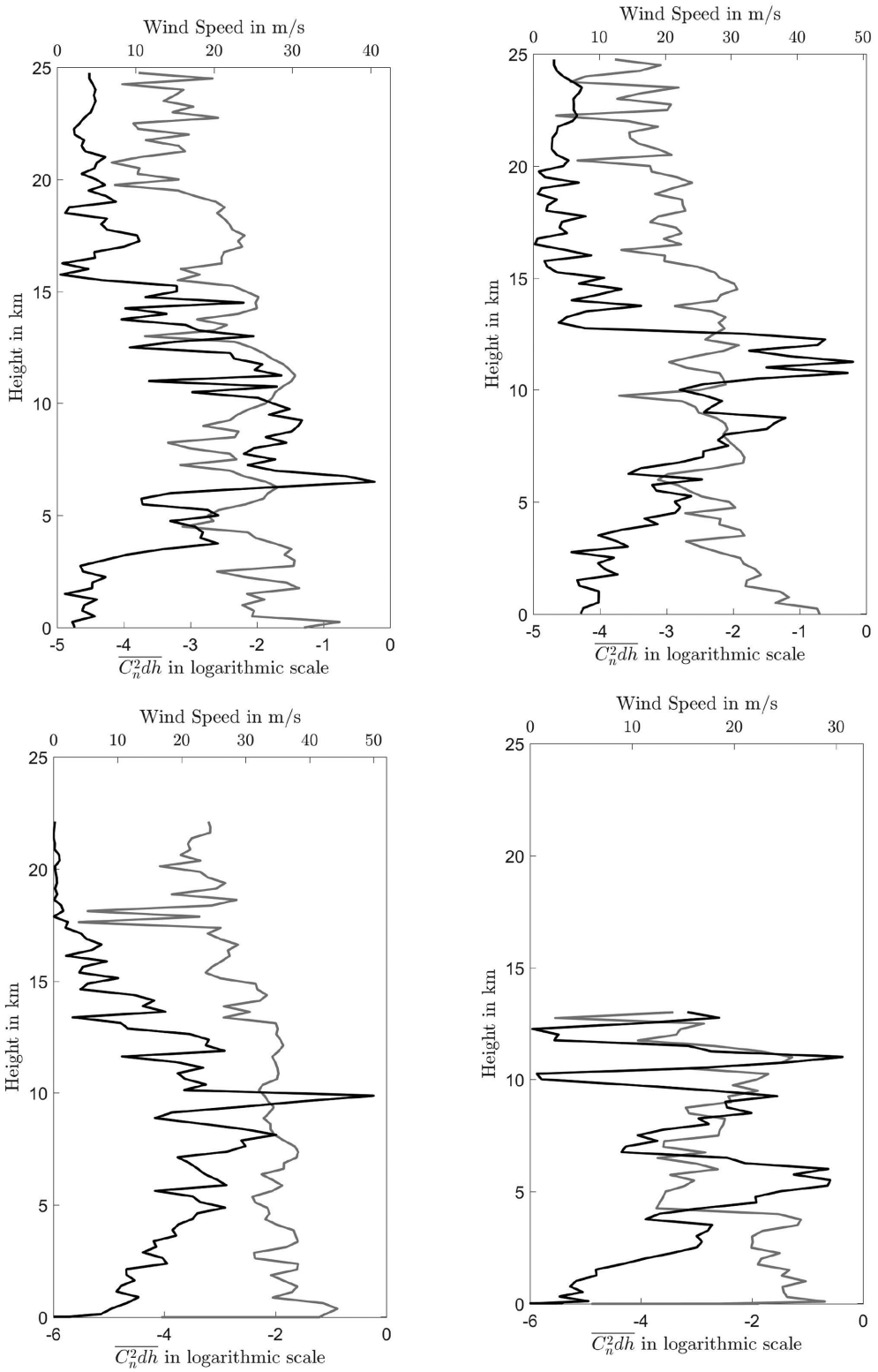

Figure 7. Typical TPs with different labels (from 1 to 4) generated by GMM trained from Paranal Data. The plot in grey is the normalized $\overline{C_{n_i}^2 dh}$ in logarithmic scale and the plot in black is the wind speed. These TPs are listed according to their labels in ascending order from left to right and from top to bottom.

(1) The characteristic time is different for different sites and different seasons. More TP data from different seasons are required to model the TP temporal variation for AO at a particular site.

(2) The characteristic time is around 2–20 min and can be longer than 30 min in some extraordinary conditions. When there is not enough TP data, we recommend to use characteristic time of 2 min for highly variable conditions and 20 min for stable conditions modelling.

(3) Due to the limited sampling rate of the TP measurement in the time domain, shorter characteristic time cannot be measured. However, as shown in Fig.5, the TP have abrupt variation over an extended period of time (200 min). These variations should be paid special attention during robustness tests of new reconstruction or control methods.

3.2 Generation of TP with temporal variation

After training with a particular TP data set, the GMM comprises several Gaussian distributions and each of them can be viewed as a generating function of TPs with a particular label. Given a random state, these Gaussian distributions can generate TPs with their labels. With the statistical results of characteristic time we obtained in Section3.1, we can generate TPs with temporal variation according to our requirements as shown in Algorithm 2.

Algorithm 2 Generation of TP with GMM

Require: :

The characteristic time δt and the total simulation time T

Ensure:

TP list **x** and the corresponding time coordinate **t** for each TP

1: Initialization of the random state $\lrcorner n$

2: Calculate the required number of TPs with different labels $N = \lceil \frac{T}{\delta t} \rceil$

3: Generate N TPs **sx** and with their corresponding labels through different Gaussian distributions with random state $\lrcorner n$

4: Process each of the generated **sx** with the following rules:
Move the minimal value of height to zero: $h_i = h_i - min(\mathbf{h})$
Normalize the $\mathbf{C_n^2}$: $C_{n_i}^2 = (C_{n_i}^2 - min(\mathbf{C_n^2}))/\sum(C_{n_i}^2 - min(\mathbf{C_n^2}))$
Calculate the absolute value of wind speed v_i: $v_i = |v_i|$
Sort all the values according to the ascending order of height and out put the TP

5: Use $\mathbf{sx_i}$ and their characteristic time δt to generate TP with temporal variation.

6: **for** $t_i \leq T$ **do**

7: $x_i = sx_i, t_i = t_{i-1} + \delta t$

8: $i = i + 1$

9: **end for**

Several artificial TPs generated by TP data from different sites are shown below: artificial La Palama TPs in Fig. 6 and artificial Paranal TPs in Fig. 7. We find that there are some TPs with strong ground layer turbulence such as TP 3 in Fig. 6 and TP 4 in Fig. 7. There are also TPs with strong turbulence in higher layers such as TP 2 in Fig. 6 and TP 1 in Fig. 7. The maximal height will change between different TPs, as shown in TP 3 of Fig. 6 with maximal height of 15 km. The wind speed reaches its maximum value around 10 km. There are some TPs with low wind speeds in the high layer, such as TP 4 in Fig. 6. In general, the TPs generated by our method have great diversity and reflect the properties of the data from Stereo-SCIDAR.

4 CONCLUSIONS

In this paper, we propose a GMM-based method that can be used to model the temporal variation of the turbulence profile. This method first uses stereo-SCIDAR turbulence profile data to train the GMM, and then obtains the characteristic time (around 2–20 minutes) of the turbulence profile through clustering by the GMM. The trained GMM can generate turbulence profile with temporal variation in accordance with the characteristic time measured on-sky.

ACKNOWLEDGEMENTS

The authors would like to thank the anonymous referee for his or her comments and suggestions which greatly improved the quality of this manuscript. This work is supported by the National Natural Science Foundation of China (NSFC)(11503018), the Science and Technology Funding Council (UK) (ST/P000541/1), the Joint Research Fund in Astronomy (U1631133) under cooperative agreement between the NSFC and Chinese Academy of Sciences (CAS) and Scientific and Technological Innovation Programs of Higher Education Institutions in Shanxi (2016033). DL acknowledges support from the UK Programme for the European Extremely Large Telescope (ST/N002660/1). OJDF acknowledges the support of STFC (ST/N50404X/1). PJ is supported by the China Scholarship Council to study at the University of Durham. Horizon 2020: This project has received funding from the European Union's Horizon 2020 research and innovation programme under grant agreement No 730890. This material reflects only the authors views and the Commission is not liable for any use that may be made of the information contained therein.

The code used in this paper is written in Python programming language (Python Software Foundation) with the package Sklearn (Pedregosa et al. 2011) and can be downloaded from http://aojp.lamost.org.

REFERENCES

Anderson J., 2016, Technical Report, Empirical Models for the WFC3/IR PSF
Andrews J. J., Price-Whelan A. M., Agüeros M. A., 2014, ApJ, 797, L32
Babcock H. W., 1953, PASP, 65, 229
Basden A., Butterley T., Myers R., Wilson R., 2007, Appl. Opt., 46, 1089
Basden A. G., Bharmal N. A., Jenkins D., Morris T. J., Osborn J., Peng J., Staykov L., 2018, SoftwareX, 7, 63
Buscher D. F., 2016, Optics Express, 24, 23566
Carbillet M. et al., 2004, in Bonaccini Calia D., Ellerbroek B. L., Ragazzoni R., eds, Proc. SPIEVol. 5490, Advancements in Adaptive Optics. pp. 637–648,
Chattopadhyay S., Maitra R., 2017, MNRAS, 469, 3374
Chen X., Li X., Sun G., Liu Q., Zhu W., Weng N., 2016, Appl. Opt., 55, 9932
Conan R., Correia C., 2014, in Adaptive Optics Systems IV. p. 91486C
Correia C., Jackson K., Véran J.-P., Andersen D., Lardière O., Bradley C., 2014, J. Opt. Soc. Am. A, 31, 101
Costille A., Fusco T., 2012, in Adaptive Optics Systems III. p. 844757
Dark Energy Survey Collaboration et al., 2016, MNRAS, 460, 1270
Gendron E., Morel C., Osborn J., Martin O., Gratadour D., Vidal F., Le Louarn M., Rousset G., 2014, in Adaptive Optics Systems IV. p. 91484N
Gilles L., Massioni P., Kulcsár C., Raynaud H.-F., Ellerbroek B., 2013, J. Opt. Soc. Am. A, 30, 898
Hao J. et al., 2009, ApJ, 702, 745
Ivezic Z. et al., 2008, preprint (arXiv:0805.2366)
Jia P., Cai D., Wang D., Basden A., 2015a, MNRAS, 447, 3467
Jia P., Cai D., Wang D., Basden A., 2015b, MNRAS, 450, 38
Jia P., Basden A., Osborn J., 2018, MNRAS, 479, 829

Kelly B. C., 2007, ApJ, 665, 1489
Kulcsár C., Raynaud H.-F., Petit C., Conan J.-M., 2012, Automatica, 48, 1939
Le Louarn M., Clare R., Béchet C., Tallon M., 2012, in Adaptive Optics Systems III. p. 84475D
Lee K. J., Guillemot L., Yue Y. L., Kramer M., Champion D. J., 2012, MNRAS, 424, 2832
Liu L.-Y., Giordano C., Yao Y.-Q., Vernin J., Chadid M., Wang H.-S., Yin J., Wang Y.-P., 2015, MNRAS, 451, 3299
Martin O., Gendron É., Rousset G., Vidal F., 2012, in Adaptive Optics Systems III. p. 84472A
Ono Y. H., Akiyama M., Oya S., Lardiére O., Andersen D. R., Correia C., Jackson K., Bradley C., 2016, J. Opt. Soc. Am. A, 33, 726
Osborn J. et al., 2014, MNRAS, 441, 2508
Osborn J., Butterley T., Perera S., Fohring D., Wilson R., 2015, in Adaptive Optics for Extremely Large Telescopes IV (AO4ELT4). p. E52
Osborn J., Wilson R., Butterley T., Morris T., Dubbeldam M., Dérie F., Sarazin M., 2016, in Adaptive Optics Systems V. p. 99091N
Osborn J. et al., 2018, MNRAS, 478 , 825
Pedregosa F. et al., 2011, J. Mach. Learn. Res., 12, 2825
Peterson J. R. et al., 2015, ApJS, 218, 14
Sarazin M., Le Louarn M., Ascenso J., Lombardi G., Navarrete J., 2013, in Esposito S., Fini L., eds, Proceedings of the Third AO4ELT Conference. p. 89
Schöck M. et al., 2009, PASP, 121, 384
Schöck M., Els S., Otárola A., Riddle R., Skidmore W., Travouillon T., 2010, in Adaptive Optics Systems II. p. 77361Z
Shang C., Oh S. P., 2012, MNRAS, 426, 3435
Shepherd H. W., Osborn J., Wilson R. W., Butterley T., Avila R., Dhillon V. S., Morris T. J., 2014, MNRAS, 437, 3568
Shin M.-S., Sekora M., Byun Y.-I., 2009, MNRAS, 400, 1897
Shin M.-S., Yi H., Kim D.-W., Chang S.-W., Byun Y.-I., 2012, AJ, 143, 65
Tokovinin A., 2004, PASP, 116, 941
Tokovinin A., Travouillon T., 2006, MNRAS, 365, 1235
Tokovinin A., Vernin J., Ziad A., Chun M., 2005, PASP, 117, 395
Tuan D. et al., 2018, in Adaptive Optics Systems IV. p. 10703
Tyson R., 2010, Principles of Adaptive Optics. CRC press
Vrieze S. I., 2012, Psychol. Methods, 17, 228
Wang L., Gilles L., Ellerbroek B., 2011, Appl. Opt., 50, 3000
Wang L., Andersen D., Ellerbroek B., 2012, Appl. Opt., 51, 3692
Xin B., Ivezić Ž., Lupton R. H., Peterson J. R., Yoachim P., Jones R. L., Claver C. F., Angeli G., 2018, preprint (arXiv:1805.02845)
Yang E.-B., Zhang Z.-B., Choi C.-S., Chang H.-Y., 2016, MNRAS, 3243
York D. G. et al., 2000, AJ, 120, 1579
Zhang L., Guo Y., Rao C., 2017, Opt. Express, 25, 4356

This paper has been typeset from a TEX/LATEX file prepared by the author.